

PACS numbers: 32.30.-r; 53.25.Os; 52.50.Jm
DOI: 10.1070/QE2005v035n07ABEH004087

Laser plume spectroscopy. 2. Graphite yttrium-stabilised and zirconium oxide targets

V.V. Osipov, V.I. Solomonov, V.V. Platonov, O.A. Snigireva, M.G. Ivanov, V.V. Lisenkov

Abstract. **Spectral and kinetic properties of a plume formed in the vicinity of a graphite and a pressed yttrium-stabilised zirconium oxide (YSZ) powder targets irradiated in air by a 10.6-μm pulsed CO_2 laser with a peak power of 1.5 – 9 kW at room temperature are studied. The plume propagated at right angles to the target surface and at an angle of 45° to the laser radiation. The spectral and kinetic characteristics of its luminescence were measured discretely along the entire length of the plume. It is shown that the YSZ plume as well as the graphite plume is a flux of nonequilibrium gaseous plasma at a temperature of about 4.7 – 3.1 kK, in which a luminescence of YO and ZrO radicals is excited.**

Keywords: *interaction of radiation with matter, laser plume, graphite target, yttrium-stabilised zirconium oxide target.*

1. Introduction

Laser-induced evaporation of solid targets of the initial material [1 – 10] is used currently for obtaining nanopowders. However, in spite of the numerous investigations of the plasma formed as a result of laser-induced evaporation, a generally accepted model has not been developed for the laser plume and the processes of condensation of the plume plasma into nanoparticles. The laser plume of a graphite target has been studied most thoroughly. In particular, it was shown in our recent publication [10] that for a CO_2 laser pulse power of the order of 10 kW, the laser plume column of the graphite target is a flux of weakly nonequilibrium plasma heated to a temperature of 10 kK as a result of the exothermic reaction of formation of C_2 molecules. This led to the conclusion that carbon nanoparticles are condensed not in a column, but predominantly in a plume cloud whose linear dimensions in the case of graphite are comparable with the size of the column.

Laser plumes of other solid targets have been studied much less intensively. The present research aims at a study of the space-resolved spectral and kinetic characteristics of the glow of a plume formed in air by the radiation of a repetitively pulsed CO_2 laser at yttrium-stabilised zirconium oxide (YSZ) targets.

V.V. Osipov, V.I. Solomonov, V.V. Platonov, O.A. Snigireva, M.G. Ivanov, V.V. Lisenkov Institute of Electrophysics, Ural Branch, Russian Academy of Sciences, ul. Amundsena 106, 620016 Yekaterinburg, Russia; e-mail: plasma@iep.uran.ru, max@iep.uran.ru

Received 24 February 2005
Kvantovaya Elektronika **35** (7) 633 – 637 (2005)
Translated by Ram Wadhwa

2. Experimental

The scheme of the experimental setup on which measurements were made was described in [10]. We used a LAERT multimode repetitively pulsed CO_2 laser [3, 9, 10]. The output beam from this laser with a cross section of 3×4 cm was focused with the help of a KCl lens of focal length 10 cm on a plane target, forming an ellipse with major and minor axes equal to 1.2 and 0.7 mm on it for an angle of incidence equal to 45°. The target was exposed to the radiation in air at room temperature. To prevent the laser pulse from falling into the same crater, the target was displaced mechanically after each pulse (except in special experiments).

Scanning of the laser plume over its length was carried out with the help of a quartz optical fibre of diameter 1 mm, which transferred the luminous flux to the entrance slit of the spectral devices. The fibre was installed in the focal plane of a quartz lens which transferred the plume image with an 8-fold magnification. Such a system ensured a spatial resolution of at least 0.25 mm.

The luminescence spectrum of the plume in the range 350 – 800 nm was recorded during a single pulse using a diffraction spectrograph and a CCD multichannel photodetector interfacing with a computer. We measured the time-integrated intensity $I(\lambda) = \int_{t_0}^{T_{\exp}} I(\lambda, t)\mathrm{d}t$, where $T_{\exp} =$ 10 ms is the exposure time of the photodetector and t_0 is the time of starting the integration, which coincides with the beginning of the laser pulse to within ±1 μs. The spectral data were averaged over 10 pulses. The error in wavelength measurements did not exceed 0.75 nm, the half-width of the instrumental function and the spectral resolution was of the order of 2 nm. The wavelength calibration of the spectrum was carried out using a spectral mercury arc lamp, while the intensity calibration was carried out using a standard incandescent lamp. The glow kinetics $I(\lambda, t)$ was measured with the help of an MCD-1 monochromator, a FEU-100 photomultiplier and a two-channel Tektronix-520A oscillograph with a 500-MHz passband. The wavelength was measured to within 2 nm by the monochromator for the same value of the instrument function. In order to determine the delay in the emergence of the laser plume emission band relative to the beginning of the laser pulse, a signal from the pyroelectric sensor of laser radiation and/or a pulse from the total radiation of the plume recorded with the help of FEK-

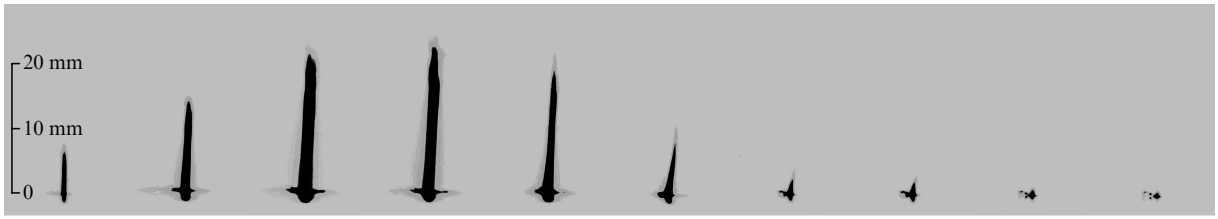

Figure 1. Photographs of the laser plume for a YSZ target (t is the instant of recording and P is the instantaneous power of laser radiation).

22 photodetector was supplied to the second channel of the oscillograph. The synchronisation error was ± 1 μs. These measurements were made under the same conditions as in [10], i.e., for a CO_2 laser pulse of energy $W_{las} = 1.4$ J, peak power $P_{max} \leqslant 9$ kW, and a duration $t_{las} = 330$ μs at the 0.1 level and with the principal peak at $t_{max} \approx 130$ μs.

In supplementary experiments, a high-speed movie camera VFU-1 was used to register the laser plume and to study its kinetics for graphite and YSZ targets upon a variation of the laser pulse power P_{max} while preserving its shape and duration.

3. Experimental results

As in the case of graphite [10], the YSZ laser plume propagated at right angles to the target surface (Fig. 1). It consisted of a cloudless column about 18 mm long for $P_{max} = 9$ kW. The diameter of the column varied insig-

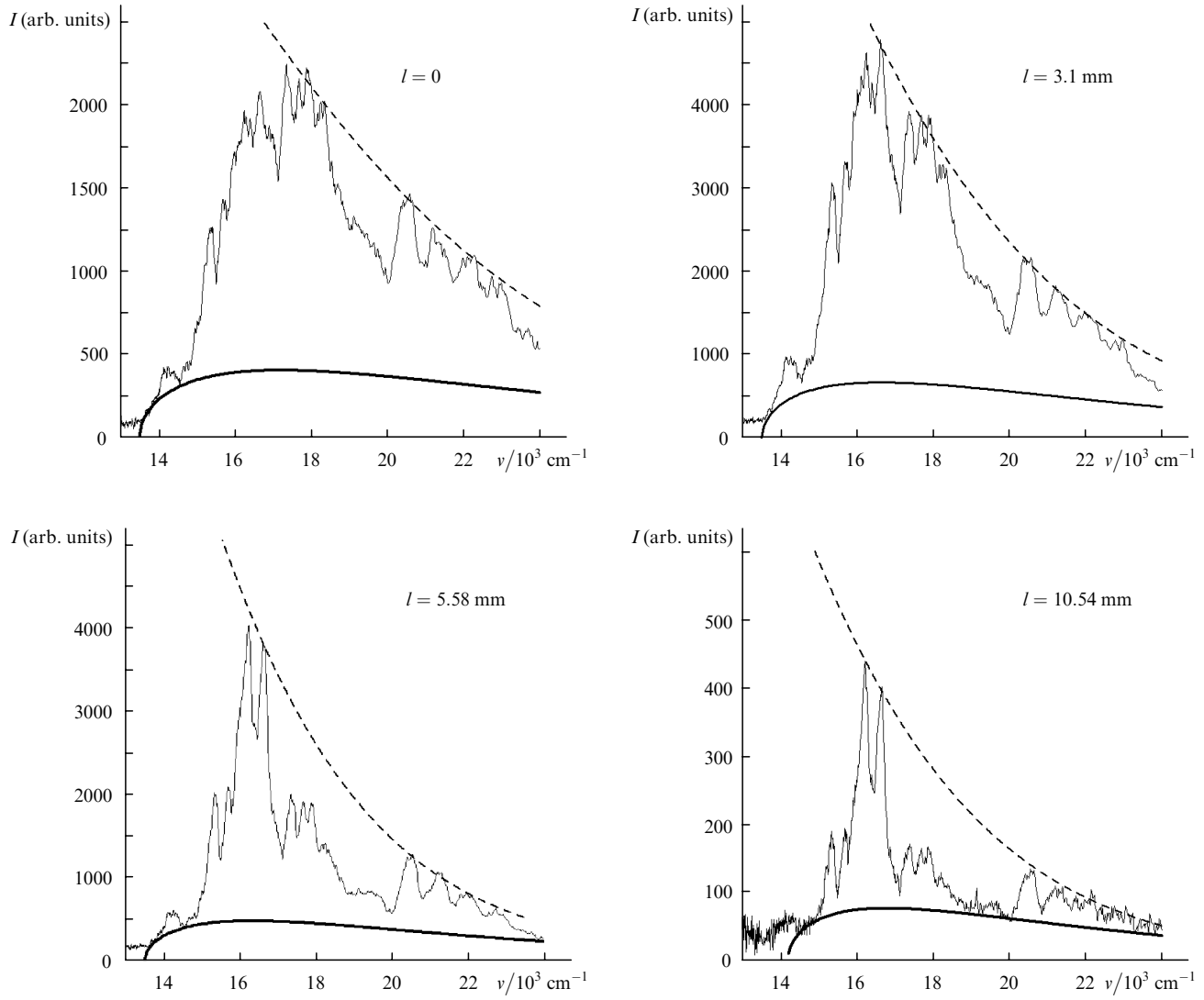

Figure 2. Emission spectra of a plume at various distances l from the target (solid curves). The thick curve is obtained as a result of recombination radiation approximation, and the dashed curve is the Wien's curve.

nificantly with the radiation power P upon an increase in the distance from the target in the interval 0.8–1.0 mm. Craters of size 1.2×0.6 mm and depth estimated at about 5–10 μm with an error exceeding 100 % were formed on the target after its irradiation. This error is due to the roughness of the target surface.

3.1 Spectral measurements

The luminescence spectra of the plume from ceramic and pressed YSZ micropowder targets were found to be identical. In contrast to the case of graphite, the spectrum for these materials is found to have a clearly manifested structure even in the vicinity of the target (Fig. 2) at a distance $l < 0.25$ mm from the target surface, but the luminescence intensity in this case is lower than in the plume column (Fig. 3). The spectral structure becomes more pronounced upon an increase in the distance from the target and three systems of the ZrO radical bands and one system of the YO radical bands are observed in this case. The intensities of all bands vary identically at different points of the plume. The intensity oscillates in the column (Fig. 3), its main peaks are observed for $l \approx 3.1$, 6.8 and 11.8 mm while the minima are observed for $l \approx 5.6$, 10.5 and 13.0 mm.

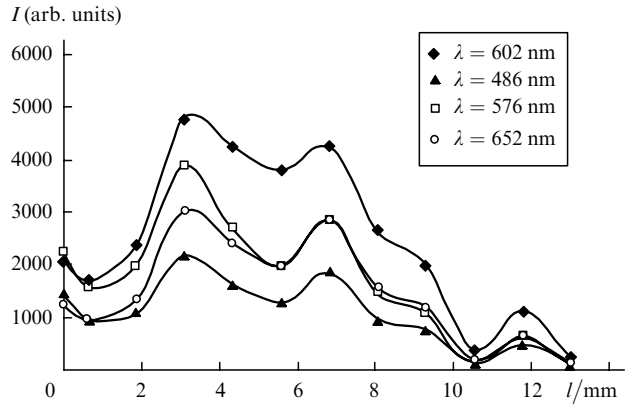

Figure 3. Dependences of the intensity I of the spectral bands of a plume on the distance l from the target.

In the blue α-system, three emission bands are observed at the $C^3\Delta \rightarrow X'^3\Delta$ vibronic transition [11] of the ZrO radical. These bands include the band of principal overtones ($\Delta v = 0$) with its centre for $\lambda = 465$ nm ($v = 21510$ cm^{-1}), the band of Stokes components ($\Delta v = -1$) for $\lambda = 486$ nm (20580 cm^{-1}), and the band of anti-Stokes components ($\Delta v = 1$) for $\lambda = 455$ nm (21980 cm^{-1}) [12]. In the yellow β-system, three bands of principal overtones of various rotational branches are observed at the $B^3\Pi \rightarrow X'^3\Delta$ transition at $\lambda = 559$, 566 and 576 nm (17890, 17670 and 17360 cm^{-1}). The Stokes components for $\lambda = 594$, 596, 604 and 607 nm (16840, 16780, 16560 and 16470 cm^{-1}) are superimposed on the YO radical band and together form a local peak at $\lambda = 600.9$ nm (16640 cm^{-1}). The anti-Stokes component is a band with its centre at $\lambda = 548$ nm (18250 cm^{-1}). In the red γ-system at the transition $A^3\Phi \rightarrow X'^3\Delta$, Stokes components are observed separately at $\lambda = 698$ and 701 nm (14330 and 14270 cm^{-1}). The remaining components of the system are superimposed on the YO radical emission band. These include the strongest principal overtones for $\lambda = 652$, 648, 638 and 635 nm (15340, 15430, 15670 and 15750 cm^{-1}) and the anti-Stokes component at $\lambda = 602$ nm (16610 cm^{-1}). Transitions from vibrational levels with $v > 1$ dominate in all emission bands of the radical ZrO.

In the spectral range investigated by us, the YO radical emits a strong band in the yellow-red spectral region at the $A^2\Pi \rightarrow X^2\Sigma$ vibronic transition with an oscillator force $f = 0.331$ [11]. In this band, i and ii series of R and Q branches are manifested [12]. The centre of the band is formed by the principal overtones ($\Delta v = 0$) for $\lambda = 613.2$ (0–0), 614.8 (1–1) and 616.5 nm (2–2) (16310, 16270 and 16220 cm^{-1}) of the iiQ band, and for $\lambda = 609.7$ (0–0) and 611.5 nm (1–1) (16400 and16350 cm^{-1}) of the iiR band. The second short-wavelength peak is formed by the principal overtones for $\lambda = 597.2$ (0–0), 598.8 (1–1) and 600.4 nm (2–2) (16740, 16700 and16660 cm^{-1}) of the iQ band on which the Stokes components of the β-system of the ZrO bands are superimposed. Components of the γ-system of ZrO are superimposed on the longwave wing of the YO band. As a result of these superpositions and the instrument effect of summation of Gaussian instrumental profiles of closely spaced spectral lines, the intensity of the entire YO band is considerably enhanced

Low-intensity bands at $\lambda = 435$ and 440 nm (22990 and 22730 cm^{-1}) and at $\lambda = 519$, 520 and 522 nm (19270, 19230 and 19160 cm^{-1}) were not identified exactly by us. They may be higher overtones of the system of bands of the ZrO radical, spectral lines of the Zr atom or oxygen ions corresponding to these wavelengths. To identify the origin of these emission bands, a higher accuracy and resolution of the spectral recordings are required.

3.2 Kinetic measurements

Within the limits of measuring errors, the delay times $t_d(l)$ of the spectral bands, recorded with the help of a monochromator and FEU-100 (Fig. 4) are identical to the delay times of integral luminescence of the plume (Fig. 5). Two peaks of luminescence intensity or a kink are observed in the kinetics of all the bands at the points in the plume where $t_d < t_{m1}$ (t_{m1} is the time of attainment of the first laser pulse peak). For $t_d > t_{m1}$ (at the points in the plume away from the target), only one intensity peak is observed. As in the case of graphite, the plume glow

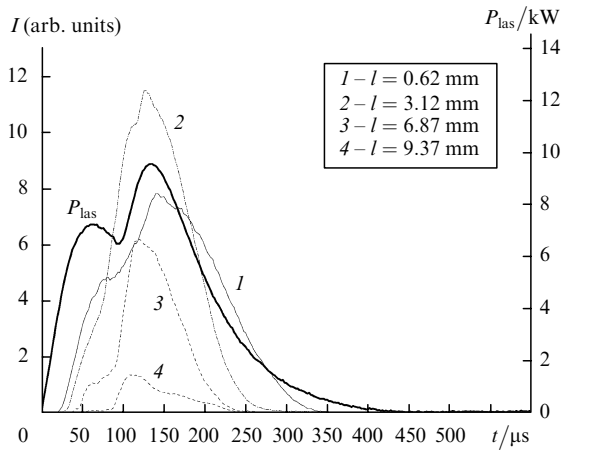

Figure 4. Kinetics $I(t)$ of the intensities of the spectral band for $\lambda = 576$ nm in the β-system of the radical ZrO at various distances l from the target surface, and of the laser pulse power P_{las} (solid curve).

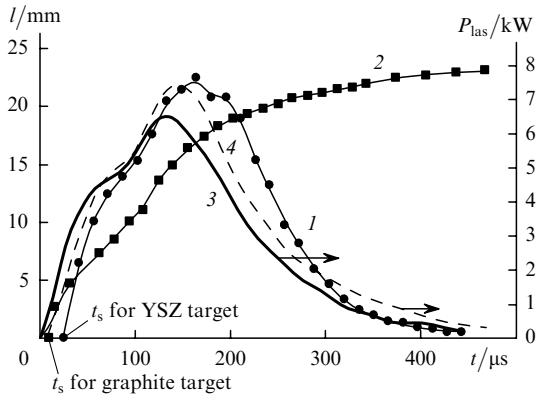

Figure 5. Space–time position of the plume heads [curves (*1*), (*2*)] and the laser pulse power [curves (*3*), (*4*)] for YSZ (*1*), (*3*) and graphite (*2*), (*4*) targets (t_s is the time of plume glow formation at the target surface).

terminates almost simultaneously (earlier) with the laser pulse. The nature of decrease in the intensities of all bands is determined by the decrease in the intensity of the laser pulse and not by the lifetime of the upper levels of optical transitions.

During recording of the luminescence kinetics of graphite and YSZ plumes with the help of FEU-100 and a high-speed movie camera VFU-1, an initial (starting) delay was observed in the emergence of the plume glow for $l = 0$ relative to the beginning of the laser pulse t_s (Figs 4 and 5). The delay time of several tens of microseconds increases upon a decrease in the laser pulse power, and the product

$$P_s t_s \approx \text{const.} \tag{1}$$

Here, $P_s = P(t_s)$ is the laser radiation power at the instant t_s. The constant (1) is equal to $(3.1 \pm 1.2)\times 10^{-3}$ and $(7.5 \pm 0.2) \times 10^{-2}$ J for graphite and YSZ, respectively. After emergence of the luminescence for $l = 0$, the length of the plume column increases to its critical value l_{max} after which the formation of a cloud begins. The dependence of the velocity $V = l/(t_l - t_s)$ (t_l is the time of emergence of the plume column head at a distance l from the target relative to the beginning of the laser pulse) of the plume column head on the laser pulse power P_{max} is described by the expression

$$V^2 = \frac{P_{max}}{a} b \tag{2}$$

with a correlation factor $r^2 \geqslant 0.99$, where $a = 0.827$ and 0.146 kg s^{-1}, $b = 1.647 \times 10^3$ and 8.427×10^3 m^2 s^{-2} are constant coefficients for graphite and YSZ, respectively.

4. Discussion of results

Unlike graphite [10], the emission spectrum of a laser plume in YSZ is highly structurised even in the vicinity of the target for $l < 0.25$ mm (Fig. 2), and the spectral luminescence intensity peak is realised in the column and not near the surface (Fig. 3). For the same parameters of the laser pulse, the glowing part of the YSZ plume is much smaller in size than in the case of a graphite target. The free electron temperature was estimated from an approximation of the continuous background (pedestal) by using the formula

$$I(v) = \frac{\alpha(hcv - \Delta E)^{1/2}}{(kT_e)^{3/2}} \exp\left(-\frac{hcv - \Delta E}{kT_e}\right), \tag{3}$$

proposed in [10] and describing the radiative recombination intensity for a Maxwell distribution of electrons over energies measured in wave numbers $v = 1/\lambda$ (solid curve in Fig. 2). In the above formula, α is the normalisation factor, T_e is the electron temperature, E is the free electron energy, and ΔE is the difference between the ionisation potential and the effective energy of a particle formed as a result of recombination. The estimate points towards a monotonic decrease in T_e from 10 kK at the target (at the tail of the column) to 7 kK at the head of the plume column in YSZ (Fig. 6). In this case, the energy difference ΔE remains constant at $\sim$13500 cm^{-1} over the entire length of the plume.

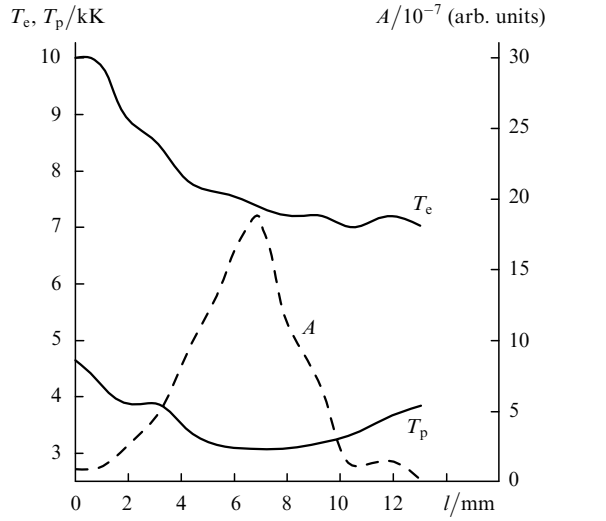

Figure 6. Dependence of the approximate values of the electron temperature T_e and plasma temperature T_p, as well as of the parameter A characterising the concentration of vapour of the substance in a YSZ plume, on the distance l from the target.

In order to estimate the plasma temperature T_p at all points of the YSZ plume, the curve enveloping the intensity peaks of the spectral bands was approximated by Wien's curve (dashed curve in Fig. 2) on the scale of wave numbers v described by the expression

$$I(v) = Av^3 \exp\left(-\frac{hcv}{kT_p}\right). \tag{4}$$

The approximation was carried out over the short-wavelength wing of the spectrum by varying the parameters T_p and A. The following expression, containing the dependence on the particle density N, is valid for the parameter A in the case of the plume plasma:

$$A = \frac{8\pi^2 e^2 h}{m} N\eta_0 \sum_i f_i, \tag{5}$$

where e and m are the electron charge and mass; f_i is the optical power of the ith oscillator of the junction lying in the spectral interval of instrument resolution; and η_0 is a coefficient characterising the properties of the optical path. For $l < 5$ mm, the correlation factor r^2 assumed values up

to ~ 0.99, for 5 mm $< l <$ 8 mm it was equal to ~ 0.87, while for large values of l it decreased to 0.83. Fig. 6 shows the results of approximation in the form of dependences of parameters T_p and A on the distance l from the target. Estimates show that the range of variation of temperature T_p is much smaller in a YSZ plume than in graphite [10]. The highest temperature is observed in the vicinity of the target surface where it attains values ~ 4.65 kK close to the boiling point of YSZ (4.573 kK) [13]. The temperature in the column decreases from 4.4 kK in the tail to its minimum value ~ 3.1 kK for $l \approx 6.8 - 7$ mm. Subsequently, this value increases to ~ 3.7 kK for $l \approx 12$ mm. In this case, a well-defined peak is observed for the parameter A at $l \approx 6.8 - 7$ mm and a low-intensity peak is formed at $l \approx 11.7 - 12$ mm (at the centre of the cloud). It follows from the above approximation and spectral analysis that matter in the YSZ plume is in the form of a weakly nonequilibrium gaseous plasma formed predominantly by molecular radicals ZrO and YO. The obtained experimental data do not lead to an unambiguous conclusion about the mechanisms of formation of molecular radicals. It is quite possible that matter vaporises from the target just in this form.

5. Conclusions

Thus, a laser plume formed under the action of a 9-kW CO_2 laser pulse on a solid YSZ target is a flux of weakly nonequilibrium plasma formed predominantly by molecular radicals ZrO and YO. The temperature of heavy particles in the plume is lower than the boiling point of YSZ. A slight increase over the boiling point is attained only in the vicinity of the target surface.

Condensation of the vaporised YSZ target matter into nanoparticles begins right in the plume column, but this process is halted by an additional heating of the column due to release of crystallisation energy. Hence the final condensation occurs apparently in the cloud at a fairly large distance (of the order of 10 mm) from the target.

An approximation formula is proposed for the velocity of laser plume in the longitudinal direction.

Acknowledgements. This work was supported by an INTAS grant (Project No. 03-51-3332) and by a grant from the Presidium of the Ural Branch of the Russian Academy of Sciences (project 'Development of Fundamental Basic Technologies Using High-Power Coherent Radiation Fluxes' under the programme of integration of the Ural and Siberian branches of the Russian Academy of Sciences.

References

1. Muller E., Oestreih Ch., Popp U., et al. *J. KONA – Powder and Particle*, (13), 79 (1995).
2. Popp U., Herbig R., Michel G., et al. *J. European Ceramic Soc*., **18**, 1153 (1998).
3. Kotov Yu.A., Osipov V.V., Ivanov M.G., et al. *Zh. Tekh. Fiz*., **72** (11), 76 (2002).
4. Dem'yanenko A.V., Letokhov V.S., Puretskii A.A., Ryabov E.A. *Kvantovaya Elektron*., **25**, 36 (1998) [*Quantum Electron*., **28**, 33 (1998)].
5. Arepalli S., Scott C.D. *Chem. Phys. Lett*., **302**, 139 (1999).
6. Lipchak A.I., Solomonv V.I., Tel'nov V.A., Osipov V.V. *Kvantovaya Elektron*., **22**, 367 (1995) [*Quantum Electron*., **25**, 347 (1995)].
7. Kokai F., Takahashi K., Kasuya D., et al. *Appl. Phys. A*, **73**, 401 (2001).
8. Nakajima K., Furusava M., Yamamoto T., et al. *Diamond and Related Materials*, **11**, 953 (2002).
9. Mesyats G.A., Osipov V.V., Volkov N.B., et al. *Pis'ma Zh. Tekh. Fiz*., **29**, 54 (2003).
10. Osipov V.V., Solomonov V.I., Platonov V.V., et al. *Kvantovaya Elektron*., **35**, 467 (2005) [*Quantum Electron*., **35**, 467 (2005)].
11. Kuznetsova L.A., Kuz'menko N.E., Kuzyakov Yu.Ya., Plastinin Yu.A. *Veroyatnosti opticheskikh perekhodov dvukhatomnykh molekul* (Probabilities of Optical Transitions in Diatomic Molecules) (Moscow: Nauka, 1980).
12. Pears R., Gajdon A. *Identification of Molecular Spectra* (London: Chapman Hall, 1963).
13. Grigoriev I.S., Meilikhov E.Z. (Eds) *Handbook of Physical Quartities* (CRS Press, Inc., Boca Raton, 1997).